NOVEL DEVICES USING MULTIFUNCTIONAL ZnO AND ITS NANOSTRUCTURES

Yicheng Lu*, Jian Zhong, Jun Zhu, Gaurav Saraf, Hanhong Chen, Ziqing Duan and Pavel Reyes
Department of Electrical and Computer Engineering, Rutgers University
94 Brett Road, Piscataway, NJ 08854-8058

H. Shen and D. Mackie
US Army Research Laboratory
2800 Powder Mill Road, Adelphi, MD 20783

R. H. Wittstruck
USA PEO IEW&S
Fort Monmouth, NJ 07703

A. Ballato
US Army CERDEC
Fort Monmouth, NJ 07703

ABTRACT

Zinc oxide (ZnO) is a promising wide band gap semiconductor. It has a direct energy band gap, E_g of 3.3eV at room temperature. ZnO can be alloyed with CdO and MgO to form the ternaries $Cd_xZn_{1-x}O$ and $Mg_xZn_{1-x}O$, extending the direct energy band from 2.8eV to 4.0eV. Through proper doping, it also can be made transparent and conductive, piezoelectric, or ferromagnetic. ZnO based single crystal nanostructures can be grown at relatively low temperature on various substrates. In this paper, we report new devices by using ZnO based multilayers and nanostructures.

We have grown high quality epitaxial ZnO and $Mg_xZn_{1-x}O$ films on r-plane sapphire substrates by metal organic chemical vapor deposition (MOCVD). The ZnO based semiconducting and piezoelectric multilayer structures are used to demonstrate various devices, including wireless SAW UV detectors and monolithically integrated tunable phase shifters.

Single crystal ZnO and $Mg_xZn_{1-x}O$ nanotips are grown on various substrates, including Si, GaN, glass, and metal, used for new light emitting diode (LED) devices. The nanotips have a diameter of ~60 nm and are oriented along the c-axis, normal to the growth plane. We have developed novel LED structures by integrating ZnO nanostructures on top of a GaN LED to enhance light extraction efficiency.

1. INTRODUCTION

ZnO and its ternary alloy $Mg_xZn_{1-x}O$, as a wide band gap semiconductor and as a multifunctional material, has been receiving increasing attention. Through proper doping and alloying, ZnO and $Mg_xZn_{1-x}O$ can be made piezoelectric (Onodera, 1997), transparent and conducting (Srikant, 1995), or magnetic (Prellier, 2003), leading to multifunctional properties that can be integrated with various devices for wide applications. ZnO can be grown as thin films or as nanostructures on a variety of substrates. ZnO is an attractive material candidate for

Report Documentation Page

Form Approved
OMB No. 0704-0188

1. REPORT DATE	2. REPORT TYPE	3. DATES COVERED
DEC 2008	**N/A**	**-**

4. TITLE AND SUBTITLE	5a. CONTRACT NUMBER
Novel Devices Using Multifunctional Zno And Its Nanostructures	5b. GRANT NUMBER
	5c. PROGRAM ELEMENT NUMBER
6. AUTHOR(S)	5d. PROJECT NUMBER
	5e. TASK NUMBER
	5f. WORK UNIT NUMBER
7. PERFORMING ORGANIZATION NAME(S) AND ADDRESS(ES) **Department of Electrical and Computer Engineering, Rutgers University 94 Brett Road, Piscataway, NJ 08854-8058**	8. PERFORMING ORGANIZATION REPORT NUMBER
9. SPONSORING/MONITORING AGENCY NAME(S) AND ADDRESS(ES)	10. SPONSOR/MONITOR'S ACRONYM(S)
	11. SPONSOR/MONITOR'S REPORT NUMBER(S)

12. DISTRIBUTION/AVAILABILITY STATEMENT
Approved for public release, distribution unlimited

13. SUPPLEMENTARY NOTES
See also ADM002187. Proceedings of the Army Science Conference (26th) Held in Orlando, Florida on 1-4 December 2008

14. ABSTRACT

15. SUBJECT TERMS

16. SECURITY CLASSIFICATION OF:			17. LIMITATION OF ABSTRACT	18. NUMBER OF PAGES	19a. NAME OF RESPONSIBLE PERSON
a. REPORT	b. ABSTRACT	c. THIS PAGE			
unclassified	**unclassified**	**unclassified**	**UU**	**8**	

ultraviolet (UV) optoelectronics, as it has a direct energy band gap (E_g) of approximately 3.3eV at room temperature, and also a free exciton binding energy of ≈60 meV. ZnO is more resistant to radiation damage than GaN (Look, 2001). Epitaxial ZnO films can be grown at ≈400°C (Gorla, 1999). High quality ZnO films show large photoconductivity. Photoconductive and photovoltaic UV detectors have been reported on polycrystalline (Fabricius, 1986) and epitaxial ZnO films (Liu, 2000; Liang, 2001). Conventional UV photodetectors have output in voltage or current; however, output in the frequency domain is preferred for the remote and wireless UV detection. Piezoelectric ZnO thin films have been used for fabricating surface acoustic wave (SAW) devices on nonpiezoelectric or weakly piezoelectric substrates. Surface acoustic wave devices have been widely used in communication systems and sensors. They have several advantages, including low power consumption, lightweight, functional versatility, and low cost. The integration of semiconducting ZnO and piezoelectric ZnO leads to novel wireless UV photodetectors using the acousto-optcal interaction in the ZnO multilayers. Furthermore, traditional SAW devices lack tunability of acoustic velocity, which would allow tuning the center frequency of the SAW filters. Such tunability is critically important in many applications, such as adaptive communications and tunable sensors. Tunable acoustic devices can also be realized by using the acoustoelectric interaction in a ZnO multilayer structure, in which a semiconductor ZnO MOS structures is integrated with a piezolectric ZnO SAW structure.

In addition to thin film growth, it is also possible to grow single crystalline ZnO nanostructures, such as nanotips on various substrates including GaN, Si, glass, and *c*-plane sapphire at low temperature (≈400°C) by metal organic chemical vapor deposition (MOCVD). ZnO nanotips possess excellent optical properties. The free excitonic emission dominates in ZnO nanotips at room temperature, which makes it suitable for optoelectronic devices. In this work, we demonstrate an integrated ZnO nanotips/GaN LED fabricated by directly growing ZnO nanotips on top of a GaN LED using MOCVD to achieve enhanced light emission efficiency. Unlike other technologies used to enhance light extraction, such as using rough surfaces and photonic crystals, this approach does not require e-beam lithography or etching, making it suitable for low cost and large scale fabrication.

2. DEVICES BASED ON MULTILAYER AND MULTIFUNCTIONAL ZnO

Surface acoustic wave devices utilize one or more interdigital transducers (IDTs) to convert acoustic waves to electrical signals and vice versa utilizing the piezoelectric effect of certain materials. SAW devices can be designed to provide quite complex signal processing functions within a single package. Due to their special advantages such as mass-producibility, low cost, small size, light weight and versatile functionality, SAW devices have been widely employed in telecommunications as bandpass and spectrum-shaping filters, convolvers, duplexers and delay lines. In addition, SAW devices are also used in Wide Area Network (WAN), Wireless Local Area Network (WLAN) communications, wireless passive identifications tags, miniature chemical/biochemical sensors. Combined with the multifunctionality of ZnO these applications can be greatly enhanced and can be made tunable and more sensitive.

2.1 SAW UV Detector: Integration of Photoconductive and Piezoelectric ZnO

The SAW UV detector is based on the acoustoelectric interaction in a ZnO multilayer structure, which consists of photoconductive ZnO and piezoelectric ZnO layers. The schematic vertical structure of a ZnO UV SAW device is shown in Figure 1(a) which consists of a piezoelectric ZnO layer on r-Al_2O_3 substrate for SAW generation, an $Mg_{0.2}Zn_{0.8}O$ buffer layer, and a semiconducting ZnO sensing layer. The ZnO/r-Al_2O_3 system possesses a high acoustic velocity and large maximum effective coupling constant obtainable with the Sezawa wave mode,

in comparison with the previously reported GaN/c-Al_2O_3 and ZnO/$LiNbO_3$ structures. The interaction of the SAW with the photogenerated carriers in the semiconducting ZnO layer results in a phase shift and an insertion loss change, as functions of light wavelength and power.

These three layers are all grown by using MOCVD. A thick piezoelectric ZnO film (≈2.0 μm) is firstly grown on r-Al_2O_3 substrates. As ZnO has a lower acoustic velocity than r-Al_2O_3, this layered system has dispersive acoustic velocity, with higher order wave modes excited at higher film thickness – frequency (hf) products. Based on the SAW simulation, the thickness is determined to ensure the excitation of the first higher order Rayleigh wave mode, the Sezawa wave mode, in the test devices below 1.0 GHz. The Sezawa wave mode is chosen as it has higher acoustic velocity, v_{SAW}, and maximum effective piezoelectric coupling, K^2_{eff}, than the base Rayleigh wave mode and the Love wave mode (Emanetoglu at al., 2001). The as-grown, unintentionally doped MOCVD ZnO shows n-type conductivity, with a carrier concentration of about 10^{17} cm^{-3} (Sheng et al., 2002). To compensate for the excess carriers in the ZnO film and ensure efficient SAW excitation, the piezoelectric ZnO layer is doped with Li to increase its resistivity to above 10^7 Ω cm (Wu at al., 2004). Then, a 50 nm thick $Mg_{0.2}Zn_{0.8}O$ buffer layer is used to isolate the semiconducting ZnO layer from the piezoelectric ZnO layer and as a diffusion barrier for Li. The semiconducting ZnO layer's thickness, h_{mesa}, is varied from 200 nm to 400 nm to determine the thickness dependence of the SAW and optical responses. After the formation of the semiconducting ZnO sensing mesa by wet chemical etching, the Al interdigital transducers are deposited and patterned on top of the piezoelectric ZnO surface. The devices are aligned parallel to the ZnO c-axis, which is in the surface plane of the $(11\bar{2}0)$ ZnO film, to generate the Rayleigh type wave modes. In the IDT region, the base Rayleigh wave mode has an estimated maximum coupling coefficient of 1.9% with a velocity of 2768 m/s, while the maximum coupling coefficient for the Sezawa wave mode is estimated to be 6% with an acoustic velocity of 5658 m/s, leading to a larger photoresponse.

When the sensing area of the UV SAW device is illuminated by UV light, the incident light will be absorbed by the semiconductor, generating electron-hole pairs. Based on the acoustoelectric interaction, these free carriers in the semiconductor layer will interact with the electric field accompanying the propagating SAW, resulting in an increased insertion loss. Additionally, a velocity reduction will occur due to piezoelectric stiffening, resulting in a phase shift and time delay across the SAW device. These SAW response changes are correlated to the light wavelength and power density of the incident light and can be used as the UV sensing information.

The ZnO SAW UV devices were tested using an HP 8753D network analyzer and Cascade Microtech probes for the RF response (the transmission parameter S_{21}). The ZnO UV SAW device was firstly evaluated under dark conditions and microscope light. Then, a 75W Xe lamp with a monochromator system was used as the UV source for detailed UV detection evaluation. Multiple UV filters were used to adjust the power density of the incident light. Two optical illumination procedures were used: illuminating the whole device surface, and only illuminating the semiconducting ZnO mesa through a shadow mask. The light wavelengths were varied from 630 nm to 300 nm. The light power density was varied from 810 $\mu W/cm^2$ to 2.32 mW/cm^2 at λ_{light} = 365 nm. I-V measurements were used to determine the change in the resistance of the mesa active layer as a function of the light wavelength and power, then correlated with the SAW photoresponse.

Figure 1(b) shows the SAW response of a UV SAW device with λ_{SAW} = 8 μm, L = 1 mm, and h_{mesa} = 300 nm, under dark and two different light power conditions (λ_{light} = 365 nm), while using a shadow mask to limit the illuminated area to the mesa. The power density of the incident light was adjusted by applying UV filters to the light beam. The base Rayleigh wave mode response is at 545.9 MHz, with an insertion loss of -67.8 dB. In

comparison, the Sezawa wave mode response is at 711.3 MHz, corresponding to v_{SAW} = 5690 m/s, with an insertion loss of -52.5 dB. The Sezawa wave insertion loss increases to -75.3 dB when the light power is 2.32 mW/cm^2, while the Rayleigh wave insertion loss is -83.3 dB. In comparison, the UV SAW detector with a 200 nm thick active region had an insertion loss of -33.8 dB for the Sezawa wave mode, due to its lower conductance. The insertion loss can also be improved by using better designed IDTs with narrower bandwidth and unidirectional transducers. When the whole device surface is illuminated, a shift in center frequency, up to 11 MHz, along with additional phase shift and insertion loss, was observed. This is due to the generation of carriers in the Li-doped piezoelectric ZnO layer under the IDTs, whose high resistivity (>10^7 Ω.cm) is insufficient to totally suppress carrier generation.

The phase shift at center frequency for the Sezawa wave mode with respect to the dark condition, as a function of light wavelength and power level, is shown in Figure 1(c). The inset shows the transmission spectrum of ZnO epi-layer grown on r-Al_2O_3 for comparison. From Figure 1(c), it can be seen that the UV SAW device response closely follows the absorption spectrum. For light wavelengths above 400 nm, the phase shift is small. The phase shift increases rapidly as the light wavelength approaches the band edge at about 372 nm. The phase shift at 365 nm for a light power of 2.32 mW/cm^2 is 107°, corresponding to a frequency shift of 1.36 MHz in an oscillator circuit, calculated for the standard oscillator circuit configuration with the SAW in the feedback path.

$$\Delta f = \frac{1}{\tau}\frac{\Delta\phi}{360^o} = \frac{1}{\frac{L_{mesa}}{v_{SAW,mesa}} + \frac{L_{IDT}}{v_{SAW,IDT}}}\frac{\Delta\phi}{360^o} \quad (1)$$

where τ is the delay time across the device, $v_{SAW,mesa}$ the acoustic velocity in the mesa region, $v_{SAW,IDT}$ the acoustic velocity in the IDT region, L_{IDT} the delay path length in the IDT region, and Δϕ the phase shift across the device. The Sezawa wave velocity in the mesa region, $v_{SAW,mesa,}$ is estimated to be 5430 m/s. This 1.36 MHz frequency shift corresponds to a 0.19% relative shift for a light power of 2.32 mW/cm^2, which compares favorably with the 0.46% relative frequency shift at 40 mW/cm^2 reported for a ZnO/$LiNbO_3$ SAW UV detector (Sharma and Sreenivas, 2003). The estimated effective coupling, k_{eff}^2, at hf = 1710 is 1.6%, calculated using the transfer matrix method (Adler, 1990). It is estimated that the maximum effective coupling that could be obtained for this structure is 3.2% at hf = 2820. Thus, device performance can be improved by operating at a higher frequency using a smaller SAW wavelength.

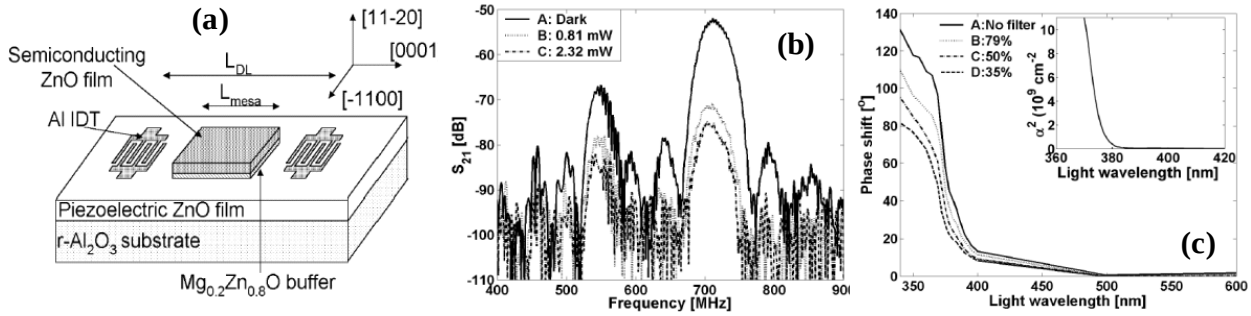

Fig. 1 (a) Device schematic of the SAW UV detector; (b) frequency response of the SAW UV detector under 365 nm light illumination, under dark, 0.81 and 2.32 mW/cm^2 conditions; (c) phase shift vs light wavelength for light power of 2.32 mW/cm^2 (no filter), 1.83 mW/cm^2 (79%), 1.18 mW/cm^2 (50%), and 0.81 mW/cm^2 (35%). The responses have been normalized for constant power with respect to 365 nm.

2.2 Voltage Controlled Phase Shifter: Integration of MIS with Piezoelectric ZnO

We have designed and demonstrated a ZnO voltage controlled multimode tunable SAW phase shifter through integration of the ZnO metal-insulator-semiconductor (MIS) structure with piezoelectric ZnO. The device is composed of a piezoelectric ZnO film/r-Al_2O_3 system and a SiO_2/semiconducting ZnO MIS structure. The acoustic velocity tunability is achieved by changing the sheet conductivity of the semiconducting ZnO channel through the gate bias. The device can be operated with both Sezawa and Love mode, which are suitable for gaseous and liquid environment sensing, respectively. Multiple sensing functions can be integrated in a single chip. Under –18 V bias, 420° and 277.3° phase shifts are achieved for Sezawa and Love mode operation, respectively. The ZnO based tunable SAW devices are expected to find broad applications in communications and in chemical/biochemical sensing.

The structure of a prototype ZnO based multimode tunable SAW device is schematically shown in Fig. 2(a). In this device, an r-Al_2O_3 substrate is used instead of the popular c-plane sapphire for the following advantages: (i) The c-axis of the ZnO film in the ZnO/r-Al_2O_3 material system is in-plane, resulting in unique anisotropic acoustic, optical, and electrical properties; (ii) The system has higher electromechanical coupling coefficients, with K^2 up to 6% for certain wave modes; and (iii) Lattice mismatch between ZnO and r-plane sapphire is less than that in ZnO/c-plane sapphire, resulting in high quality ZnO thin films.

The acoustic velocity tunability of the ZnO tunable SAW device is based on the acoustoelectric interaction between the electric field accompanying the propagating SAW and free carriers in the semiconducting channel.

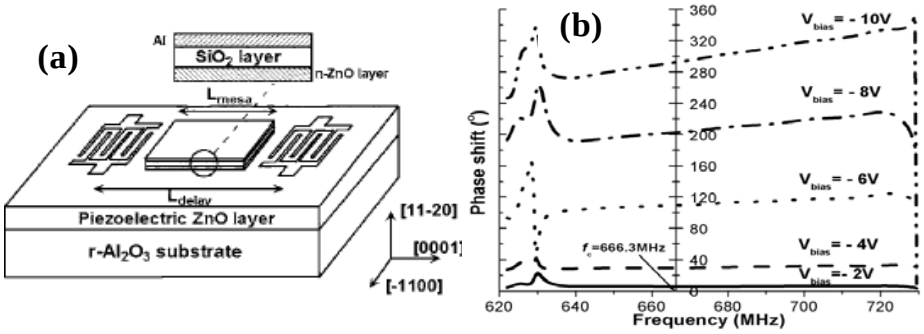

Fig. 2 (a) Schematic representation of the ZnO based tunable SAW device structure. The inset shows a cross-section view of an Al/SiO_2 /ZnO metal-insulator-semiconductor structure built on the piezoelectric ZnO.; (b) frequency spectrum of

Under zero gate bias, the sheet charge density of the semiconducting ZnO channel is high. The SAW will propagate with an initial acoustic velocity, modified by the mass-loading effect of the SiO_2/semiconducting ZnO stack and the screening effect of the gate electrode. When the electrons in the ZnO channel are depleted due to the reverse gate bias, the SAW will propagate with an open-circuit velocity v_{oc}, again modified due to the mass loading and gate electrode screening effects. When the ZnO channel is in the accumulation stage due to the forward bias, the electron density increases to a very high level, and the SAW will propagate with the slower short-circuit velocity, v_{sc}. For intermediate sheet charge densities with the change of the gate bias, the SAW's electric field will generate current in the channel, resulting in ohmic loss, and will propagate at a velocity v, which is between v_{oc} and v_{sc}. The value of v will be determined by the charge density, the effective coupling of the structure, and v_{oc}. In principle, the channel can be made either a single layer semiconductor or a two dimensional electron gas (2DEG) system, which offers larger tunable range and lower bias. In this work, single semiconducting ZnO channel and SiO_2/ZnO MIS structure are used in the tunable SAW devices.

The voltage tunable SAW phase shifters were tested using a HP 8753D network analyzer and Cascade Microtech probes for the rf response (transmission parameter S_{21}). Under different biasing voltages, the phase shifts of the measured S_{21} are calculated with respect to the reference data (no biasing). The negative biasing and DC ground is supplied by a ± 20V DC power source. I-V measurements with HP 4156 C semiconductor parameter analyzer were used to determine the resistance change of the channel layer with respect to the bias voltage. The phase shifts and attenuations of the tunable SAW device around the center frequency are evaluated under different DC biasing with respect to its reference under V_g = 0V. The center frequency of the basic Rayleigh wave mode is 528 MHz, corresponding to $v_{Rayleigh}$= 4656 m/s. In comparison, the Sezawa wave mode response is at 666.3 MHz, corresponding to v_{Sezawa}= 5330 m/s, which is close to the estimated velocity leading to the maximum coupling coefficient. Within the DC bias tunable range, both the attenuation and phase shift of the basic Rayleigh wave mode is very small. The acoustic velocity changes are located in the ppm range. Meanwhile, for the Sezawa wave mode, the velocity change resulted by DC bias is much higher due to its high coupling coefficient. The maximal phase shift is 420^o with –18 V biasing, corresponding to a 0.62% velocity change. The phase shift at the center frequency of the Sezawa wave mode with respect to the biasing changing from 0 V to –10 V is shown in Fig. 2(b). With an increase of negative biasing from 0V to –10V with –2V step, the phase shift increases continuously to 291^o. The phase transition around the center frequency (f_C ± 40MHz) is smooth with small phase noise.

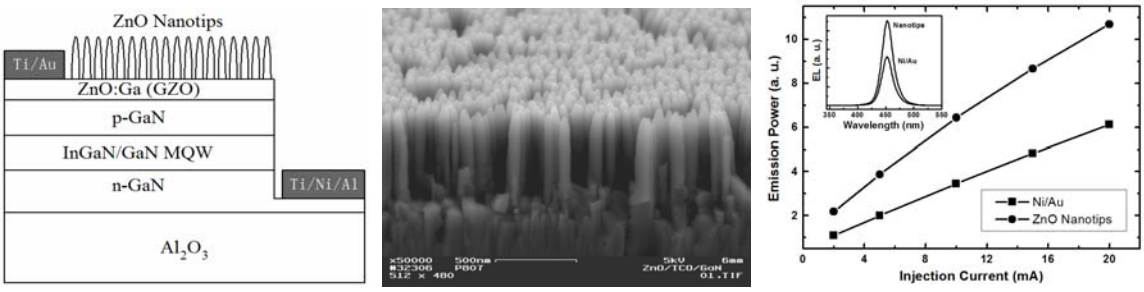

Fig. 3 (a) Schematic cross-sectional diagram of an integrated ZnO nanotips/GZO/GaN LED, (b) FESEM image of ZnO nanotips/GZO/GaN, and (c) emission power as a function of forward injection current for ZnO nanotips/GZO/GaN LED and reference Ni/Au GaN LED; inset shows EL spectra of Ni/Au p-contact GaN LED and ZnO nanotips/GZO/GaN LED at 20mA current injection.

3. INTEGRATION OF ZnO NANOTIPS WITH GaN LED

One of the major technical issues for nitride light emitting diodes (LEDs) is low external quantum efficiency, which is due to the high refractive index of GaN. Extensive efforts have been made to improve the light extraction from GaN LEDs, such as surface roughening (Fujii et al., 2004), forming photonic crystals (Oder et al. 2004), light output coupling through surface plasmons (Barnes, 1999), corrugated Bragg gratings, or using random surface texturing. Typical GaN LEDs have p-GaN layer grown on the top, in which a thick p-GaN is undesirable due to the high resistivity. Manipulation such as dry etching is often difficult in a thin layer without degrading the electrical and optical properties, and complicates the GaN LED fabrication.

In this work, an integrated ZnO nanotips/GaN LED has been investigated by directly growing ZnO nanotips on top of a GaN LED using MOCVD, to achieve enhanced light emission efficiency. In this LED structure, a Ga-doped ZnO (GZO) layer is first deposited on top of a conventional GaN LED, which serves as a transparent conductive layer to p-GaN. ZnO nanotips are then grown

on GZO coated GaN as a light extraction layer for the LED. Unlike other technologies used to enhance light extraction, such as using rough surfaces and photonic crystals, this approach does not require e-beam lithography or etching, making it suitable for low cost and large scale fabrication.

Figure 3(a) shows a schematic of an integrated ZnO nanotips/GZO/GaN LED. Conventional InGaN/GaN multiple quantum well (MQW) LED templates were grown on c-plane sapphire by MOCVD. The GaN LEDs consist of undoped and Si-doped n-type GaN base layers, InGaN/GaN MQW active region, followed by Mg-doped p-type layers. A two-step MOCVD growth technique is used for growth of the GZO film and ZnO nanotips. A FESEM picture of ZnO nanotips grown on a GZO coated GaN LED is shown in figure 3(b). They were vertically aligned with the c-axis. The nanotips have an average diameter of 60 nm at the bottom and a height of ≈400 nm. To fabricate an integrated ZnO nanotips/GZO/GaN LED, the ZnO nanotips/GZO layer was selectively etched using a diluted nitric acid. A subsequent dry etching was used to form a mesa and expose the n-type GaN layer for its n-electrode. Ti/Ni/Al and Ti/Au contacts were deposited on the exposed n-type GaN and ZnO for n- and p-electrodes, respectively. A conventional p-metal layer of Ni/Au was also deposited on a GaN LED wafer, serving as a reference. For comparison, a GZO/GaN LED without the top nanotips layer was fabricated. Light output power of LEDs was measured by a CAS 140B LED tester, and EL spectra were recorded. Figure 3(c) shows the emission power of an integrated ZnO nanotips/GZO/GaN LED as a function of forward injection current. The EL intensity from a ZnO nanotips/GZO/GaN LED has increased by 1.7 times at 20 mA current, in comparison to the Ni/Au contact GaN LED reference. The light output power of a ZnO nanotips/GZO/GaN LED is also compared with the reference GZO/GaN LED without ZnO nanotips, showing significantly increased light extraction efficiency due to ZnO nanotips. The inset of figure 3(c) shows the EL spectra of a ZnO nanotips/GZO/GaN LED and of a conventional Ni/Au GaN LED.

The enhancement in light extraction efficiency can be explained by the enhanced optical transmission and light scattering from the GaN LED and ZnO nanostructure multilayers. Based on an effective medium theory, our numerical results show that an increase of ≈20% in light extraction can be attributed to enhanced optical transmission, in comparison with a GaN layer without ZnO nanotips. A Monte Carlo simulation has been developed to calculate the variation in the effective refractive index of the nanotip layer. The result shows that the combination of surface roughening and non-uniform distribution of dielectric leads to a larger escape cone in the nanotips layer over the planar structure.

4. CONCLUSIONS

In this work we have demonstrated novel devices using multifunctional ZnO films and nanostructures. A SAW UV detector is made by integration of photoconductive ZnO and piezoelectric ZnO. The ZnO/r-Al_2O_3 system possesses a high acoustic velocity and large maximum effective coupling constant. The interaction of the SAW with the photogenerated carriers in the semiconducting ZnO layer results in a phase shift and an insertion loss change, as functions of light wavelength and power. The SAW UV detector can be used as a passive zero-power remote wireless sensor.

We have also demonstrated a voltage controlled multimode SAW phase shifter by integration of a semiconductor ZnO with a piezoelectric ZnO. The device is composed of a piezoelectric ZnO SAW structure built on an r-Al_2O_3 substrate and a ZnO MOS structure. The acoustic velocity tunability is achieved by changing the sheet conductivity of the semiconducting ZnO channel through the gate bias. We achieved a maximal phase shift of 420^o with –18 V biasing, corresponding to 0.62% velocity change. The device can be operated in both Sezawa and Love modes, which are suitable for gaseous and liquid sensing, respectively.

An integrated ZnO nanotips/GaN LED has been demonstrated. In this structure, a Ga doped ZnO (GZO) layer is first deposited on top of a conventional GaN LED, which is used as a transparent conductive layer to p-GaN. ZnO nanotips are then grown on GZO coated GaN as a light extraction layer for the LED. The light output power of a ZnO nanotips/GZO/GaN LED exhibits 1.7 times enhancement, in comparison with a conventional Ni/Au *p*-metal LED. The results promise the integration of ZnO nanotips with GaN based optoelectronic devices using epitaxial growth technology.

ACKNOWLEDGMENTS

The work has been sponsored by NSF, ARO, AFOSR, and NJ Excellence Center Program. The authors thank Dr. J. J. Song and Dr. C. K. Choi at ZN Technology for their assistance in the GaN LED fabrication.

REFERENCES

Adler, E. L. 1990: Matrix Methods Applied to Acoustic Waves in Multilayers, *IEEE Trans. Ultrason. Ferroelectr. Freq. Control*, **37**, 485-490

Barnes, W. L., 1999: Electromagnetic Crystals for Surface Plasmon Polaritons and the Extraction of Light from Emissive Devices, *J. Lightwave Technol.*, **17**, 2170-2182

Emanetoglu, N. W., Patounakis, G., Liang, S., Gorla, C. R., Wittstruck, R. H., and Lu, Y., 2001: Analysis of SAW Properties of Epitaxial ZnO Films Grown on R-Al_2O_3 Substrates", *IEEE Trans. Ultrason. Ferroelectr. Freq. Control*, **48**, 1389-1394

Fabricius, H., Skettrup, T., and Bisgaard, P., 1986: Ultraviolet detectors in thin sputtered ZnO films, *Appl. Opt.*, **25**, 2764-2767

Fujii, T. Gao, Y., Sharma, R., Hu, E. L., DenBaars, S. P., and Nakamura, S., 2004: Increase in the Extraction Efficiency of GaN-based Light-emitting Diodes via Surface Roughening", *Appl. Phys. Lett.*, **84**, 855-857

Gorla, C. R., Emanetoglu, N. W., Liang, S., Lu, Y., Wraback, M., and Shen, H., 1999, Structural, Optical and SAW Properties of Epitaxial ZnO Films Grown on (01-1 2) Sapphire by MOCVD, *J. Appl. Phys.*, **85**, 2595-2602

Liang, S., Sheng, H., Huo, Z., Liu, Y., Lu, Y., and Shen, H., 2001: ZnO Schottky Ultraviolet Photodetectors, *J. Cryst. Growth*, **225/2–4**, 110-113

Liu, Y., Gorla, C. R., Emanetoglu, N. W., Liang, S., and Lu, Y., 2000: Ultraviolet Detectors Based on Epitaxial ZnO Films Grown by MOCVD, *J. Electron. Mater.* , **29**, 69-74

Look, D. C., 2001: Recent Advances in ZnO Materials and Devices, *Mater. Sci. Eng*., B **80**, 383-387

Oder, T., N. Kim, K. H., Lin, J. Y., and Jiang, H. X., 2004: III-nitride Blue and Ultraviolet Photonic Crystal Light Emitting Diodes, *Appl. Phys. Lett.*, **84**, 466-468

Onodera, A., Tamaki, N., Jin, K., and Yamashita, H., 1997: Ferroelectric Properties in Piezoelectric Semiconductor $Zn_{1-x}M_xO$ (M = Li, Mg), *Jpn. J. Appl. Phys. Part I.*, **36**, 6008-6011

Prellier, W., Fouchet, A., Mercey, B., Simon, Ch., and Raveau, R., 2003: Laser Ablation of Co:ZnO Films Deposited from Zn and Co Metal Targets on (0001) Al_2O_3 Substrates, *Appl. Phys. Lett.*, **82**, 3490-3492

Sharma P. and Sreenivas, K., 2003: Highly Sensitive Ultraviolet Detector Based on ZnO/$LiNbO_3$ Hybrid Surface Acoustic Wave Filter, *Appl. Phys. Lett.*, **83**, 3617-3619

Sheng, H., Muthukumar, S. Emanetoglu, N. W., and Lu, Y., 2002: Schottky Diode with Ag on (11-20) Epitaxial ZnO Film, *Appl. Phys. Lett.*, **80**, 2132-2134

Srikant, V., Sergo, V., and Clarke, D. R., 1995: Epitaxial Aluminum-doped Zinc Oxide Thin Films on Sapphire: II, Defect Equilibria and Electrical Properties, *J. Am. Ceram. Soc.*, **78**, 1935-1939

Wu, P., Emanetoglu, N. W., Muthukumar, S., Chen, Y., and Lu, Y., 2004: Li Diffusion on Epitaxial (112-0) ZnO Film on r-sapphire," *J. Electron. Mater.*, **33**, 596-598